ACS APPLIED MATERIALS & INTERFACES

Research Article

www.acsami.org

Origin of Rectification in Boron Nitride Heterojunctions to Silicon

Kungen Teii,*,† Takuro Hori,† Yusei Mizusako,† and Seiichiro Matsumoto†,‡

†Department of Applied Science for Electronics and Materials, Interdisciplinary Graduate School of Engineering Sciences, Kyushu University, Kasuga, Fukuoka 816-8580, Japan

‡Exploratory Materials Research Laboratory for Energy and Environment, National Institute for Materials Science, 1-2-1 Sengen, Tsukuba, Ibaraki 305-0047, Japan

ABSTRACT: Cubic and hexagonal boron nitride (cBN and hBN) heterojunctions to n-type Si are fabricated under low-energy ion bombardment by inductively coupled plasma-enhanced chemical vapor deposition using the chemistry of fluorine. The sp^2-bonded BN/Si heterojunction shows no rectification, while the cBN/sp^2BN/Si heterojunction has rectification properties analogue to typical p−n junction diodes despite a large thickness (∼130 nm) of the sp^2BN interlayer. The current−voltage characteristics at temperatures up to 573 K are governed by thermal excitation of carriers, and mostly described with the ideal diode equation and the Frenkel−Poole emission model at low and high bias voltages, respectively. The rectification in the cBN/sp^2BN/Si heterojunction is caused by a bias-dependent change in the barrier height for holes arising from stronger p-type conduction in the cBN layer and enhanced with the thick sp^2BN interlayer for impeding the reverse current flow at defect levels mainly associated with grain boundaries.

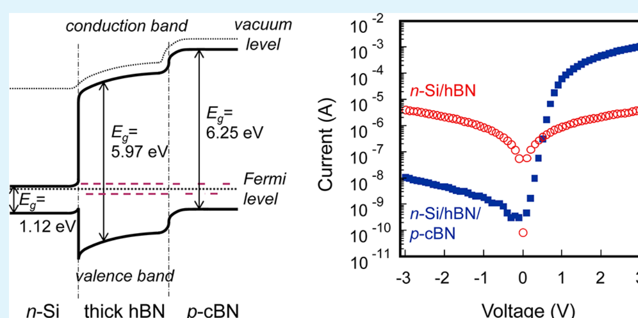

KEYWORDS: *cubic boron nitride (cBN), hexagonal boron nitride (hBN), diamond, inductively coupled plasma (ICP), plasma chemical vapor deposition, semiconductor, electronic transport, doping, diode*

1. INTRODUCTION

Cubic boron nitride (cBN) has the largest band gap energy of 6.25 eV[1] among the covalently bonded materials and is promising for development of high-power, high-voltage, and high-temperature electronic devices. Among the potential advantages of cBN over diamond is that cBN is resistant to oxidation at temperatures up to ∼1000 °C and, thus, suitable for the semiconductor that is operable at high temperatures even in air. Besides, c-BN can be doped easier as n-type as well as p-type superior to diamond. An excellent characteristic of the p−n homojunction diode using a cBN bulk single crystal, synthesized at a high pressure and a high temperature, has been demonstrated by Mishima et al.[2] For large-area and low-cost electronics, cBN should be used in the form of films.

Several groups have reported electrical transport properties of cBN films with or without addition of dopants.[3−7] However, there are only a few reports on electronic devices using cBN films dissimilar to other wide-gap semiconductor films for two main reasons. First, vapor-phase deposition of cBN films at low pressures usually requires impingement of high-energy ions on the growing surfaces, more than 50 eV depending upon the deposition techniques.[8,9] The resulting films are essentially low qualities, i.e., nanometer-sized grains, high density of structural defects, high compressive stress, and low adhesion to the substrate. This suggests that the potential outstanding properties of cBN are not available. Second, the growth of a cBN layer on foreign substrates usually follows an initial sp^2-bonded hexagonal BN (hBN) layer, consisting typically of turbostratic (tBN) and amorphous (aBN) phases, and the cBN overlayer is not always phase-pure. Although widely diverging resistivities have been reported for cBN films, the disordered sp^2BN phase has a higher resistivity by at least two orders of magnitude than the cBN phase.[10,11] This suggests that the carrier transport is strongly affected by the sp^2BN layer. Nose et al. reported clear rectification in nanocrystalline p-type cBN/sp^2BN/n-type Si heterojunctions only when the sp^2BN layer thinner than 40 nm was used.[12,13]

The introduction of the chemistry of fluorine into the chemical vapor deposition (CVD) process in a plasma jet by the work of Matsumoto and Zhang enabled one to produce high-quality cBN films with micrometer-sized grains and low compressive stress.[14,15] But the high-pressure (6.7 kPa) and high-temperature (∼1000 °C) conditions may provide only limited applicability for electronic devices. In the previous work, we demonstrated a way to deposit cBN films under low-energy ion bombardment (<50 eV) by low-pressure inductively coupled plasma (ICP)-enhanced CVD using the chemistry of fluorine.[16] The threshold ion energy and deposition temperature for cBN film deposition were reduced to a few electronvolts and ∼730 °C, respectively. The resulting film consisted of micrometer-sized grains with a crystallographic morphology and an in-depth cBN fraction up to 70 vol %.[17−19]

Received: December 14, 2012
Accepted: March 5, 2013
Published: March 22, 2013

 © 2013 American Chemical Society

The low stress enables one to deposit thick films even on WC-Co.[20] The role of fluorine has been argued as (i) preferential etching of sp^2BN phases leaving rigid cBN phase and (ii) stabilization of the growing cBN surfaces in the form of sp^3 bonding.[16] The residual fluorine atoms are dominantly bonded on the top surface of the film and, hence, little affect the bulk transport properties. It is of great value to apply those high-crystallinity cBN films to electronic devices.

In the present work, sp^2BN and cBN/sp^2BN films are deposited on n-type Si under low-energy ion bombardment by ICP-CVD using the chemistry of fluorine. Undoped cBN films intrinsically exhibit p-type conduction, which has been ascribed to the nitrogen vacancy,[4] and thus, heterostructure p–n diodes can be prepared as in refs 12 and 13. Interestingly, high rectification is observed with a large thickness (~130 nm) of the sp^2BN interlayer. We try to explain the rectifying behavior in p-type BN/n-type Si heterojunctions by introducing a concept of defect levels characteristic of microcrystalline films.

2. EXPERIMENTAL SECTION

2.1. Deposition. BN films were deposited in the high-density source region of an ICP with a three-turn helical copper antenna wound around a water-cooled silica glass tube of 50 mm in inside diameter and 350 mm in length. Inside the silica tube, a sintered BN tube 45 mm in inside diameter was suspended to suppress both impurities from the silica tube and capacitive coupling between the coil and plasma. Prior to deposition, 11 × 11 × 0.5 mm^3 n-type Si(100) substrates (~0.01 Ω^{-1} cm^{-1} at room temperature) were cleaned ultrasonically in ethanol, dipped in a HF solution, and rinsed in ethanol. The substrate was then loaded on a molybdenum holder and covered with a sintered BN frame cover. The actual coating area was about 10 mm in diameter. A mixture of He, N_2, H_2, and 10 vol % BF_3 diluted in He at flow rates of 80, 10, 10, and 18 sccm, respectively, was used. The radio-frequency plasma power at 13.56 MHz and total pressure were kept at 1 kW and 40 Pa. The substrate was heated by plasma without a heater and its temperature was measured to be 1000 ± 20 K with an infrared pyrometer. The electron density near the substrate measured with a Langmuir probe was around 3 × 10^{11} cm^{-3}. A positive direct-current bias (V_s) was applied to the substrate in reference to the grounded stainless steel chamber. The mean ion-impact energy was controlled by the sheath potential (V_{sheath}), which is defined by a difference between the plasma potential and the substrate bias V_s. The value of V_{sheath} measured with an emissive probe decreased from 45 V to a few volts or less with increasing V_s from 0 to +100 V due to an upward shift of the plasma potential.[16,21,22] An sp^2BN layer was formed for V_{sheath} above ~40 V, while a cBN layer was formed on an initial sp^2BN layer for V_{sheath} below ~40 V.[16]

2.2. Characterization. For structural characterization of BN films, Fourier transform infrared spectroscopy (FTIR, Perkin Elmer Spectrum 100) and glancing-angle x-ray diffraction (XRD, Rigaku RINT-2000) were used. For electrical characterization of BN/Si heterojunctions in a diode configuration, four-point Ni dot electrodes with 1.5 mm-diameter were fabricated on the films by magnetron sputtering. Al was deposited on the back of the Si substrates by vacuum evaporation, and it was connected to a copper plate extraction electrode with silver paste. The samples were annealed at 573 K in vacuum (10^{-4} Pa), and then current-voltage (I–V) measurements were done with a current/voltage source (Keithley 2400) for the measurement temperature (T_M) from room temperature (298 K) up to 573 K in vacuum (10^{-4} Pa).

3. RESULTS AND DISCUSSION

3.1. FTIR Spectra of BN Films. FTIR absorption spectra of the sp^2BN (sample A) and cBN/sp^2BN (sample B) films measured in transmittance mode are shown in Figure 1. The deposition condition and film thickness of samples A and B are listed in Table 1. Sample A was deposited with V_{sheath} = 45 V, while sample B was deposited by switching V_{sheath} from 45 to 25 V to control the thickness of the sp^2BN interlayer.

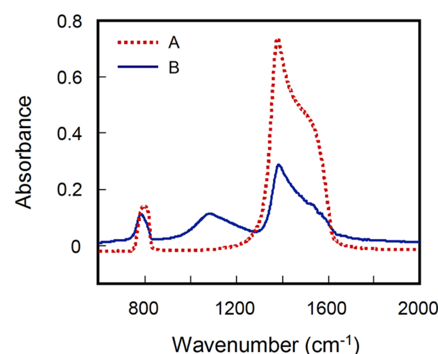

Figure 1. FTIR absorption spectra of samples A and B measured in transmittance mode.

Table 1. Deposition Time and Film Thickness of Samples A and B

	time (min)		thickness (nm)[a]	
	V_s = 0 V	V_s = +30 V	sp^2BN	cBN
sample A	20	0	320	0
sample B	10	15	130	50

[a]The uncertainty arising from the in-plane nonuniformity is estimated within ±15 nm.

In Figure 1, the absorption peaks at around 780 and 1380 cm^{-1} are attributed to the in-plane transverse optical (TO) mode of sp^2BN and a mixture of the in-plane TO and two-phonon out-of-plane modes of sp^2BN, respectively. The absorption peak at around 1080 cm^{-1} is attributed to the restrahlen band of cBN, which appears only in sample B. The film thickness for each phase is estimated from the values of absorbance of cBN and sp^2BN by using the IR absorption coefficients of cBN (17 000 cm^{-1}) and sp^2BN (22 000 cm^{-1}) for our films.[23] The full width at half maximum (fwhm) of the sp^2BN peak at around 780 cm^{-1} is 52 and 58 cm^{-1} for samples A and B, respectively. The same tendency is also observable from the sp^2BN peak at around 1380 cm^{-1}. This indicates slightly higher crystallinity of the sp^2BN phase in sample A. The apparent crystal size calculated from XRD patterns was a few nanometers, and around 5 nm for sp^2BN and cBN phases, respectively. The small apparent crystal size is due to a high density of structural defects.[19]

3.2. Electrical Characterization of BN/Si Heterojunctions. The I–V characteristics of samples A and B for the variation of T_M are shown in Figure 2a and b. Sample A shows no rectification such that the reverse current lies in the same order of magnitude as the forward current at any T_M. This is in agreement with ref 12, but different from ref 24 which showed clear rectification at room temperature. Since the carrier mobility and concentration in the sp^2BN layer are fundamentally low, the I–V characteristic resembles that of a metal–insulator–metal system, where the current behavior is limited by the leakage current flow. Sample B shows clear rectification at low T_M. The rectification ratio at 298 K is 1 × 10^5 at ±3 V, which is higher than 4 × 10^4 at ±3 V reported previously.[12,13] With an increase in T_M, the reverse current increases largely from 6.1 × 10^{-7} A cm^{-2} (298 K) to 1.1×10^{-1} A cm^{-2} (573 K)

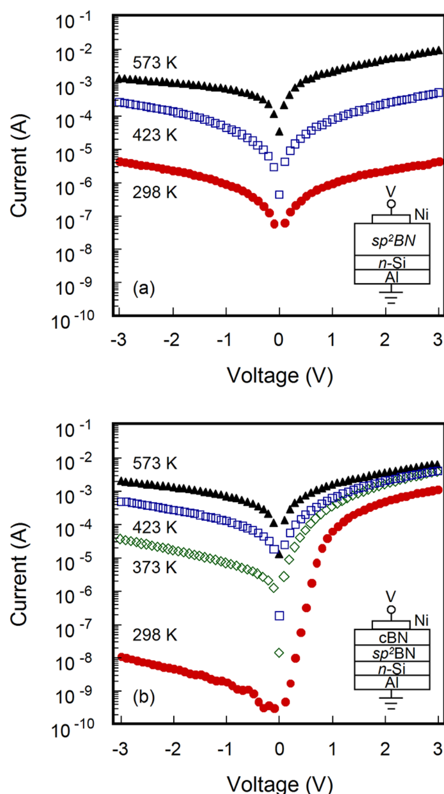

Figure 2. $I-V$ characteristics of samples A (a) and B (b) for the variation of T_M. (inset) Schematics of the electrode configuration.

at −3 V due mainly to increasing thermal activation of intrinsic carriers in the Si substrate, while the forward current increases by six times only. Consequently, the rectification ratio decreases down to the order of unity at 573 K. A faint rectification at T_M above 473 K would be due to the Schottky barrier presumably at the electrode/film contact. Further study of other several samples revealed that the smaller thickness of the sp^{2}BN layer tended to increase the reverse current and thereby decrease the rectification ratio.

The Shockley diode equation gives the $I-V$ characteristic of an ideal p−n junction diode:[25]

$$I = I_s\{\exp[q(V - IR_s)/n_i k_B T_M] - 1\} \quad (1)$$

where I_s is the reverse saturation current, R_s is the series resistance, q is the elementary electric charge, and n_i is the ideality factor. At low bias voltages where R_s can be assumed equal to zero, n_i is determined from the slope of the linear region in a plot of $I/\{1 - \exp(-qV/k_BT_M)\}$ versus V. Figure 3 shows the plots of $I/\{1 - \exp(-qV/k_BT_M)\}$ at 298 K against forward bias voltage V. The plots of both the forward and reverse currents for sample A produce straight lines with an identical slope corresponding to n_i = 7.6 below 0.4 V. The plot of the forward current for sample B produces a straight line corresponding to n_i = 2.4 below 0.8 V, while that of the reverse current is not in a straight line due partly to the low signal-to-noise ratio. High values of n_i are generally attributed to interface states and resistance, series resistance, and barrier inhomogeneity, etc. The lower value of n_i for sample B than that for sample A is attributed to the smaller thickness of the sp^{2}BN layer which acts as the depletion layer. A thinner depletion layer allows sharper rise in current when applying the same bias voltage.

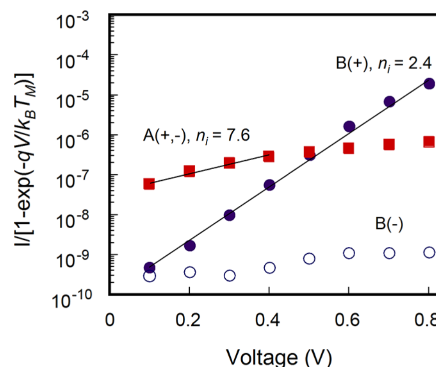

Figure 3. Plots of $I/\{1 - \exp(-qV/k_BT_M)\}$ at T_M = 298 K as a function of V for the forward (+) and reverse (−) currents of samples A and B.

Figure 4 shows the plots of I_0/T_M^2 against reciprocal T_M, the so-called Richardson plots, where I_0 is the extrapolated

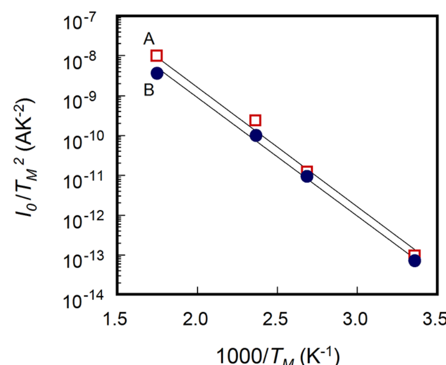

Figure 4. Plots of I_0/T_M^2 as a function of reciprocal T_M for samples A and B.

intercept at 0 V, based on the thermionic emission theory. The linearity indicates that the forward current injection barrier is independent of T_M and, hence, defect-dominated. The linear fit to the data results in the interface barrier potential $\Phi_{B(IV)}$ = 0.59 eV for sample A and $\Phi_{B(IV)}$ = 0.55 eV for sample B. Thus, the values of $\Phi_{B(IV)}$ for samples A and B are almost identical and fundamentally low. In disordered interfaces, an $I-V$ barrier $\Phi_{B(IV)}$ corresponds to a lower barrier height through which the forward current passes. The low current injection barriers obtained above are principally associated with current paths via various defect states at the disordered interfaces between the Si substrate and sp^{2}BN layer.

The Arrhenius plots of the forward and reverse currents at each bias voltage against reciprocal T_M produced straight lines with different slopes, depending on the bias voltage. The linearity suggests that the carrier transport is apparently limited by thermal excitation of carriers. The apparent activation energy derived from the linear fit to the plots is shown as a function of bias voltage in Figure 5. For sample A, the activation energy at reverse bias is slightly higher than that at forward bias, but the value remains in a narrow range of 0.30−0.40 eV. For sample B, it is clearly seen that the activation energy is constantly around 0.60−0.65 eV at reverse bias and, then, decreases drastically down to around 0.08 eV by switching the bias voltage to forward. The variation of activation energy confirms that the barrier height for carriers depends more upon

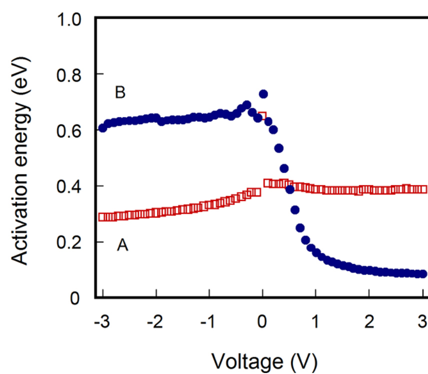

Figure 5. Apparent activation energy for conduction as a function of bias voltage for the forward (+) and reverse (−) currents of samples A and B.

the polarity of the voltage and less upon the magnitude of the voltage itself, similar to typical p−n junction diodes.

The current flow in our samples is apparently bulk-limited, not electrode-limited, as the forward and reverse currents tended to vary with the in-depth cBN fraction and the film thickness. The plots of the forward and reverse current densities (J) at 298 K divided by the electric field (E) versus $E^{1/2}$ are shown in Figure 6, as the test for bulk-limited Frenkel−Poole emission:[26,27]

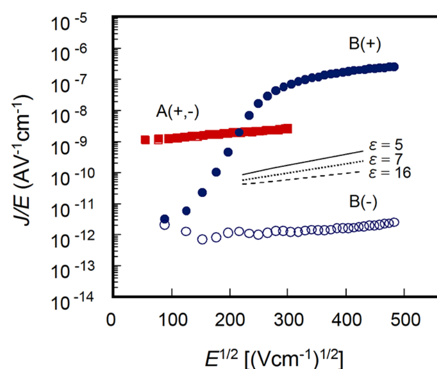

Figure 6. Plots of J/E at T_M = 298 K as a function of $E^{1/2}$, as the test for bulk-limited Frenkel−Poole emission, for the forward (+) and reverse (−) currents of samples A and B. The solid, dotted, and broken lines are the theoretical slopes for ε = 5, 7, and 16, respectively, derived from eq 2.

$$J \propto E \exp[-q(\phi_B - \sqrt{qE/\pi\varepsilon\varepsilon_0})/k_B T_M] \quad (2)$$

where ϕ_B is the trap potential (barrier height), ε_0 is the permittivity of free space, and ε is the dielectric constant of the material. The value of E was calculated here assuming that the bias voltage was applied solely to the resistive sp^2BN layer. Frenkel−Poole emission generally refers to field-enhanced thermal excitation of trapped electrons into the conduction band and is often observed in disordered materials with a high density of localized states at the Fermi level and in the band tails. In Figure 6, the plots of the forward and reverse currents for sample A produce straight lines with an identical slope nearly over the whole E range. The plots of the forward and reverse currents for sample B produce straight lines only at high E above ~80−90 kV cm^{-1}, where the two slopes approach the same as those for sample A. This indicates that at high E, the forward and reverse currents for sample B are governed by Frenkel−Poole emission in the sp^2BN layer. The trap potential ϕ_B derived from the extrapolated intercept at 0 V of the slope is ~0.4 eV for sample A, and ~0.3 eV (forward) and ~0.6 eV (reverse) for sample B. The dielectric constant ε derived from the slopes at high E is around 16, which is higher than the static value of approximately 5 and 7, typical of single crystal hBN and cBN, respectively.[28,29] This is unreasonable as the high-frequency value (e.g., ~4.5 for single crystal cBN[29]) appropriate for the Frenkel−Poole model is usually lower than the static one. This contradiction would perhaps be explained by the anomalous Frenkel−Poole effect, which introduces a factor of 2 in the exponent of eq 2 and reduces the dielectric constant to a quarter of the measured one (for our case, ~4), with the assumption of shallow neutral traps and deep donor levels.[30] However, further study of other several samples revealed that the Frenkel−Poole mechanism is not always applicable for reverse currents in cBN/sp^2BN/Si heterojunctions because of variation of the slope with deposition conditions.

3.3. Origin of Rectification in cBN/sp^2BN/Si Heterojunctions. The predicted band diagram of the cBN/sp^2BN/Si heterojunction in thermal equilibrium is depicted in Figure 7.

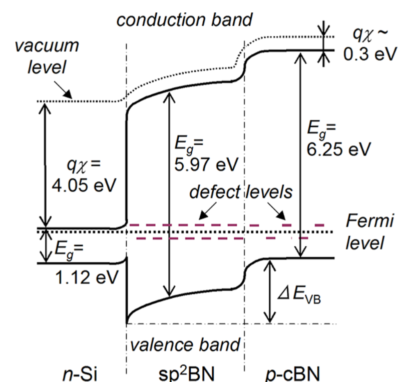

Figure 7. Predicted energy-band diagram of the cBN/sp^2BN/Si heterojunction in thermal equilibrium. E_g is the band gap, and q_χ is the electron affinity.

Band gaps of 5.97[31] and 6.25 eV[1] are adopted for sp^2BN and cBN, respectively. The electron affinity of ~0.3 eV for sp^2BN and cBN is based on our ultraviolet photoemission measurement,[18,19] while that of 4.05 eV for Si is taken from ref 25. The position of the Fermi level for cBN is lower than that for sp^2BN, and the depletion layer spreads dominantly in sp^2BN because of the low carrier concentration in sp^2BN compared to both cBN and Si. ΔE_{VB} is a difference in the valence band maximum between sp^2BN and cBN arising from a difference in the position of the Fermi level. At forward bias, ΔE_{VB} is reduced down to negative by biasing, and then, the major carriers (holes) in cBN are drifted along the applied field and injected into the Si. At reverse bias, ΔE_{VB} is increased by biasing, so that the holes in cBN are no longer injected into the Si due to the increasing barrier height. This is shown by the clear rectification in Figure 2b and the bias-dependent activation energy in Figure 5, basically consistent with the previous work.[13] However, the behavior of reverse current cannot be explained adequately only by the change in ΔE_{VB}.

In microcrystalline films, various structural defects in grain boundaries including dangling bonds and distorted arrangement of atoms can introduce a number of defect levels into the

band gap most likely near the Fermi level and thereby generate major and minority carriers and trap sites. The number density of such defect levels in disordered sp^2BN may be higher than that in crystalline cBN. However, sp^2BN is more resistive than cBN because of the lower mobility in disordered sp^2BN network. At reverse bias, the minority carriers (electrons) in the BN can be transported along localized states at the defect levels, perhaps by Frenkel−Poole emission or some thermally-activated process and injected into the conduction band of the Si, thus increasing the reverse leakage current. For sample A, both the forward and reverse currents are governed by defect-induced conduction, that is, the leakage current flow. For sample B, the reverse current is limited to be low enough due to a low electron concentration in cBN and has a tendency to increase by a decrease in thickness of the sp^2BN layer, which serves as the resistive medium and impedes the reverse current flow, consistent with our observed results.

It is remarkable that high rectification was obtained with the sp^2BN layer about 130 nm thick, which is much larger than below 40 nm reported previously.[12,13] This could be due to a fundamental difference in the ion impact energy for film deposition. The low ion energy in our method results in less dense films as indicated by about two-thirds of the IR absorption coefficients for sp^2BN and cBN phases compared to those with the high ion energy.[23] It would allow easier transport of carriers via defect levels. In fact, the resistivity of our sp^2BN films is lower by at least two orders of magnitude than that with the high ion energy.[13] On the other hand, the behavior of reverse current was better described with defect levels mainly associated with grain boundaries. A thicker sp^2BN interlayer is expected to enhance rectification by decreasing the reverse current, as long as the forward current is kept high. Higher rectification should be achieved by optimizing both forward and reverse current flows in the sp^2BN layer.

5. CONCLUSIONS

Electrical transport properties of polycrystalline BN/Si p−n heterojunctions fabricated by ICP-CVD using the chemistry of fluorine have been examined at temperatures up to 573 K. No rectification was observed with the sp^2BN layer only, while a rectification ratio of the order of 10^5 was achieved at room temperature with the cBN/thick sp^2BN double layer. For both the sp^2BN/Si and cBN/sp^2BN/Si heterojuctions, the temperature-dependent $I-V$ characteristics suggested that thermal excitation dominates the carrier transport process on the basis of the ideal diode equation and Frenkel−Poole emission model at low and high bias voltages, respectively. The potential barrier height for holes arising from higher p-type conduction in the cBN layer was responsible for rectification in the cBN/sp^2BN/Si heterojunction. Moreover, the behavior of reverse leakage current was explained in terms of the transport of minority carriers at defect levels in the resistive sp^2BN interlayer.

AUTHOR INFORMATION

Corresponding Author

*E-mail: teii@asem.kyushu-u.ac.jp.

Notes

The authors declare no competing financial interest.

ACKNOWLEDGMENTS

This work was supported in part by Funding Program for Next Generation World-Leading Researchers (NEXT Program) from the Cabinet Office, Government of Japan, and Industrial Technology Research Grant Program in 2008 from the New Energy and Industrial Technology Development Organization (NEDO) of Japan.

REFERENCES

(1) Watanabe, K.; Taniguchi, T.; Kanda, H. *Phys. Stat. Sol., A.* **2004**, *201*, 2561−2565.

(2) Mishima, O.; Tanaka, J.; Yamaoka, S.; Fukunaga, O. *Science* **1987**, *238*, 181−183.

(3) Ronning, C.; Dreher, E.; Feldermann, H.; Gross, M.; Sebastian, M.; Hofsäss, H. *Diamond Relat. Mater.* **1997**, *6*, 1129−1134.

(4) Litvinov, D.; Taylor, C. A., II; Clarke, R. *Diamond Relat. Mater.* **1998**, *7*, 360−364.

(5) Nose, K.; Oba, H.; Yoshida, T. *Appl. Phys. Lett.* **2006**, *89*, 112124.

(6) Yin, H.; Pongrac, I.; Ziemann, P. *J. Appl. Phys.* **2008**, *104*, 023703.

(7) Ying, J.; Zhang, X. W.; Yin, Z. G.; Tan, H. R.; Zhang, S. G.; Fan, Y. M. *J. Appl. Phys.* **2011**, *109*, 023716.

(8) Mirkarimi, P. B.; McCarty, K. F.; Medlin, D. L. *Mater. Sci. Eng., R Rep.* **1997**, *21*, 47−100.

(9) Weidner, S.; Geburt, S.; Milz, S.; Ye, J.; Ulrich, S.; Ronning, C. *Diamond Relat. Mater.* **2012**, *22*, 88−91.

(10) Sugino, T.; Kawasaki, S.; Tanioka, K.; Shirafuji, J. *Appl. Phys. Lett.* **1997**, *71*, 18−20.

(11) He, B.; Zhang, W. J.; Zou, Y. S.; Chong, Y. M.; Ye, Q.; Ji, A. L.; Yang, Y.; Bello, I.; Lee, S. T.; Chen, G. H. *Appl. Phys. Lett.* **2008**, *92*, 102108.

(12) Nose, K.; Tachibana, K.; Yoshida, T. *Appl. Phys. Lett.* **2003**, *83*, 943−945.

(13) Nose, K.; Yang, H. S.; Yoshida, T. *Diamond Relat. Mater.* **2005**, *14*, 1297−1301.

(14) Matsumoto, S.; Zhang, W. J. *Jpn. J. Appl. Phys. Part 2* **2000**, *39*, L442−L444.

(15) Zhang, W. J.; Jiang, X.; Matsumoto, S. *Appl. Phys. Lett.* **2001**, *79*, 4530−4532.

(16) Teii, K.; Yamao, R.; Yamamura, T.; Matsumoto, S. *J. Appl. Phys.* **2007**, *101*, 033301.

(17) Teii, K.; Matsumoto, S.; Robertson, J. *Appl. Phys. Lett.* **2008**, *92*, 013115.

(18) Teii, K.; Yamao, R.; Matsumoto, S. *J. Appl. Phys.* **2009**, *106*, 113706.

(19) Teii, K.; Matsumoto, S. *J. Appl. Phys.* **2012**, *111*, 093728.

(20) Teii, K.; Matsumoto, S. *ACS Appl. Mater. Interfaces* **2012**, *4*, 5249−5255.

(21) Teii, K.; Hori, M.; Goto, T. *J. Appl. Phys.* **2001**, *89*, 4714−4718.

(22) Teii, K.; Matsumoto, S. *J. Appl. Phys.* **2007**, *101*, 013302.

(23) Teii, K.; Hori, T.; Matsumoto, S. *Thin Solid Films* **2011**, *519*, 1817−1820.

(24) Kimura, C.; Yamamoto, T.; Sugino, T. *Diamond Relat. Mater.* **2001**, *10*, 1404−1407.

(25) Sze, S. M. *Semiconductor Devices: Physics and Technology*, 2nd ed.; Wiley: New York, 2001.

(26) Frenkel, J. *Phys. Rev.* **1938**, *54*, 647−648.

(27) Sze, S. M.; Ng, K. K. *Physics of Semiconductor Devices*, 3rd ed.; Wiley: New York, 2006.

(28) Karim, M. Z.; Cameron, D. C.; Hashmi, M. S. J. *Surf. Coat. Technol.* **1993**, *60*, 502−505.

(29) Gielisse, P. J.; Mitra, S. S.; Plendl, J. N.; Griffis, R. D.; Mansur, L. C.; Marshall, R.; Pascoe, E. A. *Phys. Rev.* **1967**, *155*, 1039−1046.

(30) Simmons, J. G.. *Phys. Rev.* **1967**, *155*, 657−660.

(31) Watanabe, K.; Taniguchi, T.; Kanda, H. *Nat. Mater.* **2004**, *3*, 404−409.